Title No. 121-M21

Statistical Process Control of Fiber-Reinforced Concrete Precast Tunnel Segments

by C. Pleesudjai, D. Patel, K. A. Williams Gaona, M. Bakhshi, V. Nasri, and B. Mobasher

Statistical process control (SPC) procedures are proposed to improve the production efficiency of precast concrete tunnel segments. Quality control test results of more than 1000 ASTM C1609/C1609M beam specimens were analyzed. These specimens were collected over 18 months from the fiber-reinforced concrete (FRC) used for the production of precast tunnel segments of a major wastewater tunnel project in the Northeast United States. The Anderson-Darling (AD) test for the overall distribution indicated that the data are best described by a normal distribution. The initial residual strength parameter for the FRC mixture, f^D_{600}, is the most representative parameter of the post-crack region. The lower 95% confidence interval (CI) values for 28-day flexural strength parameters of f_1, f^D_{600}, and f^D_{300} exceeded the design strengths and hence validated the strength acceptability criteria set at 3.7 MPa (540 psi).

A combination of run chart, exponentially weighted moving average (EWMA), and cumulative sum (CUSUM) control charts successfully identified the out-of-control mean values of flexural strengths. These methods identify the periods corresponding to incapable manufacturing processes that should be investigated to move the processes back into control. This approach successfully identified the capable or incapable processes. The study also included the Bootstrap Method to analyze standard error in the test data and its reliability to determine the sample size.

INTRODUCTION

Precast segmental tunnel lining is an important component of tunnel infrastructure needed for the operation of tunnel boring machines (TBMs) and providing permanent ground support. The functionality of tunnels depends on the structural and durability performance of these lining systems as protective barriers against large overburden loads and complex geotechnical exposure conditions. The precast linings are suitable for tunneling in both soft ground and fractured hard rock and serve as initial and final support. They are used as the dominant lining option due to their efficiency, construction speed, and economics in comparison to conventional cast-in-place lining systems.[1]

Steel fiber-reinforced concrete (SFRC) is known for improving concrete's ductility by bridging cracks and resisting their propagation and opening. The ductility and strength offered by steel fibers allow a partial or complete replacement of traditional reinforcing steel cages. In many structural applications, using a hybrid design with steel fiber and reinforcing bar has shown significant structural and economic advantages.[2-4] It is also known that the dispersion of steel fibers, especially in the reinforcement cover region, improves the durability and delays the onset and extent of corrosion.[5] Steel fiber use in tunnel linings has considerably increased during the past decade.[6] Moreover, fiber reinforcement mitigates the bursting and spalling of concrete at segment joints in both circumferential joints (under TBM thrust jack forces) and longitudinal joints (under hoop forces due to embedment loads).[7,8] Also, segment joint cracks are inevitable due to joint misalignment under strict production and construction tolerances.[9] By reinforcing the edges or corners, SFRC further resists premature deterioration of the segments during the construction phase.

The random nature of short fibers used as primary or secondary reinforcement requires a reliable set of estimates for quality control (QC) during manufacturing. The residual strength offered by the fiber-reinforced concrete (FRC) is a function of the number of fibers crossing the cracked section and is often used as a measure of variability in the post-crack performance.[10,11] Other parameters include the strength, geometry, type, and orientation of fibers in a bridged cracked section, as well as interfacial shear strength during fiber pullout,[12] structural size, and the test setup.[13-16] The treatment of FRC as an isotropic material is not directly applicable because cracking is inevitable under certain conditions and the residual strength of an FRC member depends on the variability of the material.[17] The contribution of steel fibers to the residual strength is measured by using the load-deflection curve obtained from the ASTM C1609/C1609M flexural tests[18] to back-calculate the apparent tension and compression stress-strain responses.[19] The idealized stress-strain relationships derived from the load-deflection response, allowing for the design of sections with different sizes, shapes, and reinforcements.[20]

RESEARCH SIGNIFICANCE

The use of TBMs in the construction of tunnels using precast FRC segments has resulted in significant economic advantages in terms of quality, economic aspects, and speed of construction. Due to the interlocking nature of the precast segments, QC and tolerance aspects of section dimensions, strength, and ductility affect the serviceability significantly. Unanticipated problems with durability and watertightness

could lead to costly repair and significant downtime of essential infrastructure elements. Better identification of the trends in data and understanding the variations causing outlier samples through statistical process control (SPC) provide acceptable risk levels and are important aspects of the design process. Monitoring the potential problems before field installation, when combined with the necessary number of samples tested, is also an important aspect of process control.

The purpose of this paper is to address the QC aspects of the flexural data by the proposed SPC procedures adopted in daily tests on the FRC used in different production cycles during the segment fabrication phase of a major wastewater tunnel project. The objective is to correlate the interrelationship of the measured properties with the acceptance criteria and to determine if, by monitoring the deviations observed, the knowledge could be identified to avoid out-of-control trends and control the production schedule. Furthermore, an extensive investigation into the minimum sampling requirements for ASTM C1609 testing was conducted by the Bootstrap Method approach to obtain statistical data from a limited number of random samples. The findings provide valuable insights into the variability of results obtained through ASTM C1609 and, consequently, propose minimum sampling requirements. By adhering to these recommended sampling guidelines, FRC users can minimize the number of tests, leading to considerable time and cost savings while ensuring the reliability of FRC properties.

EXPLORATORY BACKGROUND DATA

The data set used for this study was obtained from the construction production data of South Hartford Conveyance and Storage Tunnel over 18 months from mid-2018 to late 2019.[21,22] Project specification required portland cement Type I/II, calcareous aggregates, and air content of 3 to 6%. Specified properties include minimum compressive strengths of 14 and 45 MPa (2000 and 6500 psi) at stripping time and 28 days, respectively; maximum water-cementitious materials ratio (w/cm) of 0.35; silica fume content of 5% of cementitious materials; maximum aggregate size of 19 mm (3/4 in.); and maximum chloride-ion penetrability of 1000 coulombs. The reinforcement was a double hooked-end steel fiber with a tensile strength of 1800 MPa (260 ksi), length of 60 mm (2.36 in.), and an aspect ratio of 80, with a minimum dosage of 40 kg/m³ (67 lb/yd³). These specifications were used satisfactorily in a preconstruction trial and the mixture presented in Table 1. As a part of the QC requirements, ASTM C1609 beam specimens were tested daily during the production days. Multiple specimens were tested at two curing ages of formwork stripping and 28 days. The design parameter (residual flexural strength) was 2.3 MPa (340 psi) for stripping age. For serviceability design, a parameter of 3.7 MPa (540 psi) was specified as characteristic 28-day flexural strength at the first crack (f_1) and residual flexural strength at a deflection of 0.75 mm (0.03 in.) as f^D_{600} when tested following the test procedures.[18] Using these data, the equivalent tensile strength values were calculated from these specifications using back-calculation methods.[11] The limit state design strength criteria at 28 days

Table 1—Concrete mixture proportions of precast tunnel segments

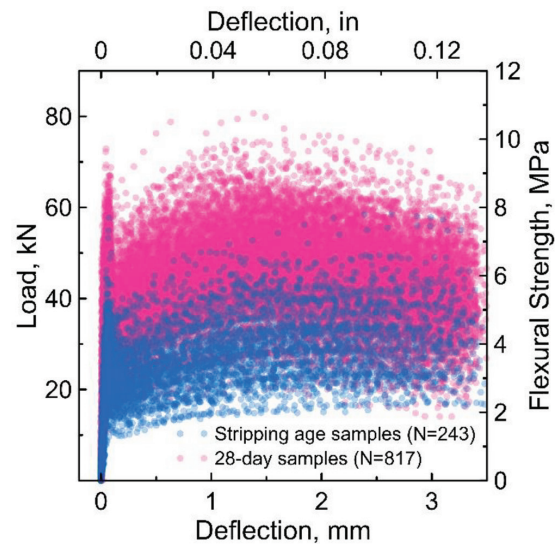|	SI units, kg/m³	Imperial units, lb/yd³
Total cementitious materials	373.8	630
Portland cement Type I/II	355.1	598.5
Silica fume (SF)	18.7	31.5
Fine aggregate	842.5	1420
Coarse aggregate	1154.6	1946
Water	131.2	221
High-range water-reducing admixture	2.1	3.6 (57 fl oz)
Steel fiber	42.1	71
Unit weight	2545	4291
w/cm	0.35	
SF/cm	5%	
Steel fiber-volume fraction (V_f)	0.54%	
Air content	3.9%	

Fig. 1—Scatter plot of four-point bending ASTM C1609 tests at stripping age and 28 days.

were specified as 4 MPa (580 psi) characteristic residual flexural strength at a deflection of 1.5 mm (f^D_{300}) or 3 mm (f^D_{150}). This characteristic strength was specified as 2.5 MPa (360 psi) for stripping age. The total number of ASTM C1609 test results accounted for 1060 specimens, with 243 specimens tested at stripping age and 817 specimens at 28 days during the period from June 2018 to October 2019. Figure 1 shows the load-deflection results of the standard four-point bending (ASTM C1609[18]) test for both the stripping age (a few hours up to 1 day) and 28 days of curing. The variation in the range of the test data for the entire production cycle is noted. After the initial loading and first cracking, a nonlinear response is expected that is demonstrated by either deflection softening or hardening in the post-crack zone. Most test results showed a sudden drop after the first crack load. The maximum level of post-cracking load at stripping age
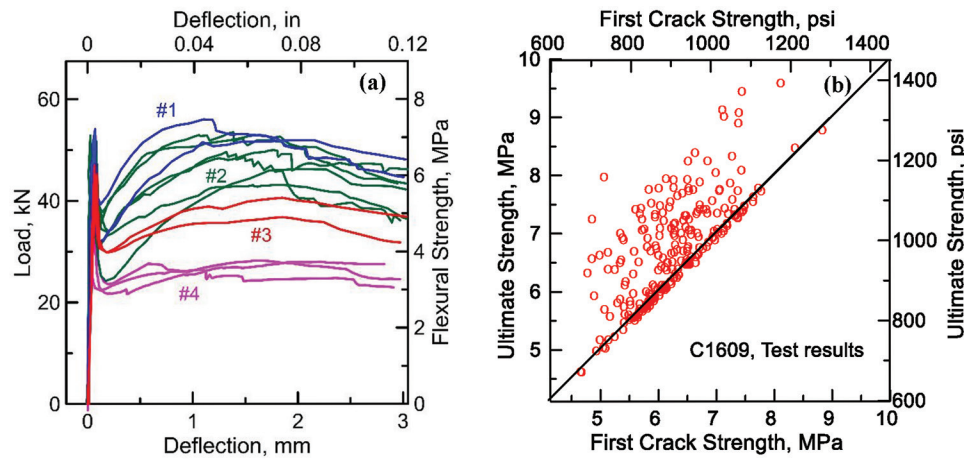
Fig. 2—(Left) Representative samples of different response categories; and (right) correlation of first crack strength (f$_l$) with peak strength (f$_p$) at 28 days, showing evidence of deflection hardening.

occurred near a deflection of 2 to 3 mm (0.08 to 0.12 in.), while the maximum residual load observed in 28-day specimens was in the early stage of deflection—that is, 1 to 2 mm (0.04 to 0.08 in.). The enhanced behavior and post-crack hardening could be attributed to improved bond strength between the fibers and cementitious matrix after 28 days of curing. Moreover, the scatter plot of 28-day specimens ranges from a minimum of 14 kN (3108 lb) to a peak load of 77 kN (17,232 lb), which, in terms of equivalent flexural stress, is 1.87 to 10.27 MPa (271 to 1489 psi), respectively, representing approximately 1.4 times the scatter at stripping age (refer to Fig. 1).

The load-deflection responses were categorized and separated into several ranges covering the deflection-softening to deflection-hardening responses. Figure 2(a) shows these four ranges as representative plots of behavior that span the post-cracking responses. Group 1 represents typical specimens in the deflection hardening. Between Groups 2, 3, and 4, the response of FRC gradually changes toward deflection softening such that, as shown in Fig. 2(a), Group 4 represents a constant stress deflection-softening. It is reasonable to expect that within each range the results will vary as well. Figure 2(b) shows the correlation of first crack strength (f$_l$) with the peak strength (f$_p$) of the 28-day specimens, indicating that for most samples, the flexural peak strength exceeds the first crack strength. The points falling on the 1:1 line exhibit deflection softening, and those above the line are deflection hardening. Most of the specimens show deflection hardening.

Descriptive measures of statistics

The ASTM C1609[18] test measures the apparent flexural strength at first crack, peak strength, and at certain prescribed deflection values by using Eq. (1). Parameter P is the applied load; L is the span length; and b and h are the width and depth of the beam section, respectively. Typical parameters are b = 152 mm (6 in.), h = 152 mm (6 in.), and L = 457 mm (18 in.). The apparent residual flexural stress, f, is calculated using the elastic section modulus at deflections corresponding to $L/600$ (0.75 mm [0.03 in.]), $L/300$ (1.5 mm [0.06 in.]), and $L/150$ (3 mm [0.12 in.])
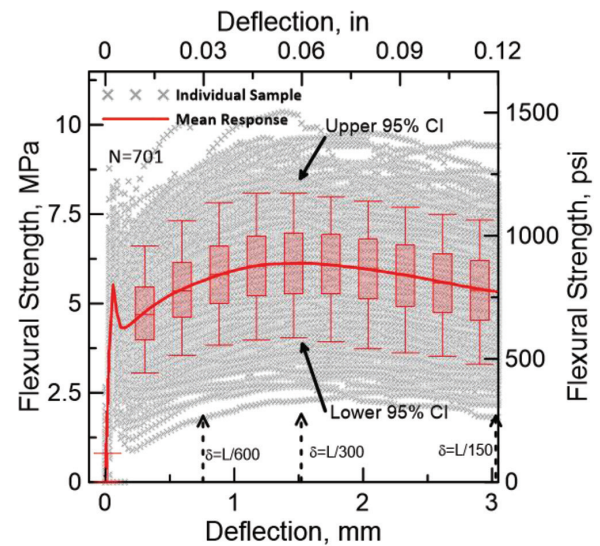

Fig. 3—Scatter plot of all data with mean curve and box and whisker plot of flexural response of individual data for 28-day specimens.

$$f = \frac{PL}{bh^2} \quad (1)$$

The individual load-deflection response of specimens up to a 3 mm (0.12 in.) deflection level was used for the evaluation of the descriptive statistics. Figure 3 shows the mean value of apparent flexural stress and its box and whisker plot through the range of deflections. Only the 28-day results are presented in Fig. 3. Individual 28-day test results that failed to meet the deflection level of $L/150$ were eliminated from pooled data, resulting in a total of 701 data sets. The whiskers extend a distance of 95% two-sided confidence interval (CI) from the ends of the box, while the box encloses the interquartile range with a lower line at the first quartile (Q1) and an upper line at the third quartile (Q3). The line drawn through the box in the middle is the 50th percentile. The variation of residual strength observed on the box and whisker plot at different deflection levels was not significant throughout the entire testing range. The data beyond the whiskers were flagged as outliers. Table 2 presents with N = 701 the descriptive statistics, including mean, standard

Table 2—Descriptive statistics of flexural strength parameters and deflections

Descriptive statistic	First crack strength, f_1, MPa (psi)	Deflection at f_1, δ_1, mm (in. × 10^{-3})	Peak strength f_P, MPa (psi)	Deflection at f_P, δ_P, mm (in. × 10^{-3})	f^D_{600}, MPa (psi)	f^D_{300}, MPa (psi)	f^D_{150}, MPa (psi)	$f^D_{e,150}$, MPa (psi)
Mean	6.36 (923)	0.068 (2.67)	6.79 (985)	0.78 (30.65)	5.65 (819)	6.1 (886)	5.32 (772)	5.60 (813)
SD	0.88 (128)	0.025 (0.99)	1.00 (146)	0.85 (33.34)	1.19 (173)	1.22 (177)	1.23 (179)	1.10 (159)
Minimum	3.33 (483)	0.12 (0.48)	3.31 (480)	0.012 (0.48)	1.78 (259)	2.29 (332)	1.82 (264)	2.10 (306)
Maximum	9.51 (1379)	2.89 (11.38)	10.32 (1497)	3.28 (129)	8.96 (1300)	9.90 (1436)	9.40 (1364)	9.00 (1306)
95% lower CI	4.87 (707)	0.031 (1.24)	5.17 (750)	0.049 (1.93)	3.73 (541)	3.98 (577)	3.23 (469)	3.70 (536)
95% upper CI	7.72 (1119)	0.095 (3.74)	8.52 (1235)	2.25 (88.56)	7.66 (1111)	8.07 (1171)	7.27 (1055)	7.33 (1064)

deviation (SD), minimum, maximum, and 95% two-sided CI for major flexural parameters. These parameters include the flexural strength at the first crack (f_1); the peak stress (f_P); residual flexural strengths at $L/600$ (f^D_{600}), $L/300$ (f^D_{300}), $L/150$ (f^D_{150}); the equivalent flexural strength ($f^D_{e,150}$); and deflections at first crack and peak strength (δ_1 and δ_P). The equivalent flexural strength ($f^D_{e,150}$) of ASTM C1609 is the average stress value obtained from the absorbed energy of the beam—that is, the area under the load-deflection curve from deflection 0 to $L/150$ (3 mm [0.12 in.]).

The mean flexural strength at the first crack (f_1) was 6.36 MPa (923 psi) with 95% two-sided CI values of 4.87 and 7.72 MPa (707 and 1119 psi), respectively. While many of the specimens demonstrated deflection softening, the deflection-hardening response was more noticeable with the mean peak strength (f_P) of 6.79 MPa (985 psi) and its 95% two-sided CI values of 5.17 and 8.52 MPa (750 and 1235 psi). The mean value of first-crack deflection (δ_1) was 0.068 mm (2.67×10^{-3} in.) with 95% two-sided CI values determined as 0.031 mm (1.24×10^{-3} in.) and 0.095 mm (3.74×10^{-3} in.). Because of the deflection-hardening effect, mean peak-strength deflections (δ_P) were higher at 0.78 mm (30.65×10^{-3} in.) as well as the 95% two-sided CI values at 0.049 mm (1.93×10^{-3} in.) and 2.25 mm (88.56×10^{-3} in.). Among residual strength parameters, f^D_{300} had the highest mean value of 6.10 MPa (886 psi), followed by f^D_{600} and f^D_{150} of 5.65 (819 psi) and 5.32 MPa (772 psi). This is also evident from the shape of the stress-deflection curve with a vertex around the middle of the curve near $L/300$ (1.5 mm [0.06 in.]) deflection range.

The SD and coefficient of variation (COV) of residual strengths f^D_{600}, f^D_{300}, and f^D_{150} range from 1.19 to 1.23 MPa (173 to 179 psi), 20 to 23%, respectively, and are almost identical. All of minimum, maximum, and two-sided 95% CI values for these residual strength parameters are within 2 to 13% of each other, except for the minimum value of f^D_{300}, which is 28% higher than the minimum value of f^D_{600}. The similarity of residual flexural strength parameters indicates that no significant differences among the parameters are observed. The mean value of ASTM C1609's equivalent flexural strength ($f^D_{e,150}$) was calculated based on the total toughness (area under the load-deflection curve) and compared with the three residual parameters. Results indicate that f^D_{600} is the most representative residual strength parameter of the post-crack region, especially with less than a 1% difference from the mean value of $f^D_{e,150}$. In addition,

Table 3—p-value and AD values of different probability distribution functions

	Normal		Weibull		Lognormal	
	AD	p-value	AD	p-value	AD	p-value
f_1	0.529	0.176	2.346	<0.010	3.372	<0.005
f^D_{600}	0.487	0.223	2.584	<0.010	3.149	<0.005
f^D_{300}	0.441	0.289	1.137	<0.010	5.033	<0.005
f^D_{150}	0.333	0.509	0.540	0.186	5.209	<0.005

the box and whisker plot in Fig. 3 presents similar variations through the range of deflections, with some results identified as outliers. Using a 95% lower confidence bound for f_1, f^D_{600}, and f^D_{300}, 28-day strength values of the FRC mixture were 4.87, 3.73, and 3.98 MPa (707, 541, and 577 psi). All these values validate and exceed the design parameters. To classify this FRC mixture according to *fib* Model Code (MC) 2010,[23] characteristic residual strengths were determined at crack mouth opening dimensions (CMOD) of 0.5 mm (0.02 in.) (f_{R1k}) and 2.5 mm (0.1 in.) (f_{R3k}). Because the CMOD was not directly measured, the deflection-CMOD relationship proposed by Conforti et al.[24] was used, which resulted in f_{R1k} as the characteristic stress f at a deflection of 0.38 mm (0.015 in.) and f_{R3k} as the characteristic stress f at a deflection of 1.72 mm (0.068 in.). Because *fib* MC 2010[23] requires the characteristic parameters (and not the mean) corresponding to a probability of 5% failure, the 95% lower confidence bound curve was used for determination. f_{R1k} and f_{R3k} were obtained as 3.05 and 3.88 MPa (435 and 563 psi), respectively. f_{R1k} represents a strength interval of 3 MPa (435 psi) and f_{R3k}/f_{R1k} =1.29 represents the letter *d*, which refers to a strength ratio class of $1.1 \leq f_{R3k}/f_{R1k} \leq 1.3$. Therefore, the FRC mixture according to *fib* MC 2010 is classified as 3*d*.

Flexural strength distribution of 28-day specimens

Three distributions—including the normal, Weibull, and lognormal—were tested to determine their applicability to adequately describe the ASTM C1609 first crack and residual strengths results. The p-values of the strength distributions were used to determine the appropriateness of the distribution. Results are reported in Table 3 for the 95% confidence interval as the level of hypothesis acceptance. If the p-value was lower than or equal to 0.05, the given distribution function was rejected from the null hypothesis, indicating that it was not suitable for describing the data. Table 3 shows that the normal distribution is acceptable for the flexural strength

distribution of the first crack, f^D_{600}, f^D_{300}, and f^D_{150}. This observation shows a good correlation with another study by Dean et al.[25] The highest p-value of a normal distribution was in flexural strength at $L/150$, accounting for 0.509, and the lowest was 0.176 in first crack strength. The Weibull distribution is only applicable for residual strength at $L/150$ (f^D_{150}), while the lognormal distribution function was rejected for all groups. The smallest value of Anderson-Darling (AD) test also compared the fit of several distributions to determine the suitability. The AD value of normal distribution in Table 3 is significantly lower than the lognormal and Weibull distributions. This confirmed that a normal distribution is the best fit for ASTM C1609 experimental data, with the normal distribution function addressing f_1 and residual flexural strength f^D_{150} with a normal probability function shown in Fig. 4. The narrow bell-shaped curve of f_1 in this figure confirmed the lower SD compared to f^D_{150}, as previously presented in Table 2.

STATISTICAL PROCESS CONTROL

A methodology to evaluate FRC quality is by using SPC. This procedure for QC is beneficial for producers, contractors, owners, and construction management. The ASTM C1609 test is known to have a high variation in the data, as measured by the COV, which can range from 2 to 25%.[15,24,26] The residual strength variability is attributed to the concrete mixture formulation and type, size, strength, dosage, and geometry of the fiber. In particular batches, the rheology affects the fiber orientation, placement direction, compaction procedures, self-compaction, vibrating-compaction, and the formwork wall-side effect.[15] Regardless of how carefully maintained and well-designed a mixture is, a natural level of variability always exists. Nevertheless, such natural variability is considered small and should not shift the mean values of FRC strength or result in out-of-control events. In the context of design, the natural variability in residual strength can be addressed by limiting the design criteria at a certain CI level when population characteristics were assumed unchanged. Variability due to temperature and climatic conditions affecting the curing and conditioning of the test specimens, mixing, batching, and placing machinery, or operator errors are considered as assignable causes of variation that may shift the mean and SD of the process. These production uncertainties must be evaluated and eliminated to confirm that FRC product properties are applicable for the design framework. SPC is a tool for early detection of spurious shifts and provides the necessary detection and warning for out-of-control FRC manufacturing. Cumulative sum (CUSUM) and exponentially weighted moving average (EWMA) are two well-known SPC methods to capture the production variability. These methods are fundamentally similar in monitoring the variations of the time-based data. The difference is that the CUSUM approach uses a constant weight factor for all the data, while the EWMA applies an exponential weight factor, giving recent observations more weight than the older data set. Laungrungrong et al.[27] suggested that by combining the control charts such as the CUSUM and EWMA with the run chart, small shifts (1.5 SD or less) in the concrete production line can be monitored,
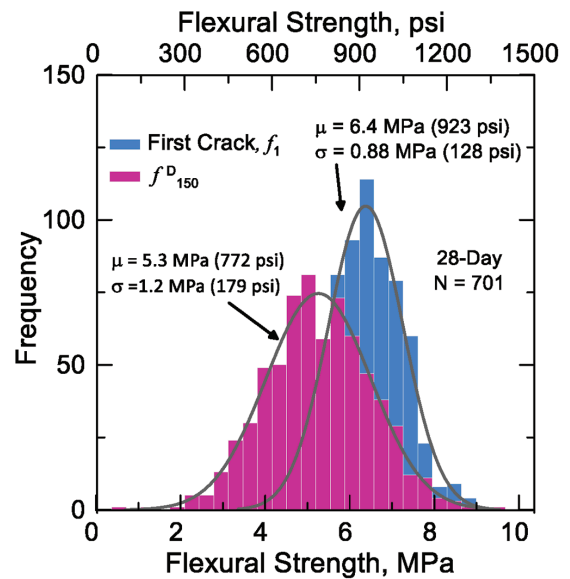

Fig. 4—Probability distribution plot and normal probability distribution function of first crack strength f_1 and residual flexural strength f^D_{150}.

thus allowing concrete producers and precast plant manufacturers to identify the problems beforehand.

The production variability investigated in this section is applicable only for the specimens at 28 days, and the ultimate deflection has to meet $L/150$ (3 mm [0.12 in.]). Therefore, the total number of individual ASTM C1609 tests is 701 out of 843 samples that were studied in this section. This SPC procedure was applied to the first crack strength, f_1, the ultimate strength, f_P, and the residual strengths f^D_{600}, f^D_{300}, and f^D_{150}. The interpolation of run charts and control charts is described to provide insight into distinguishing between QC and SPC and comparing signals in CUSUM and EWMA methods.

Run chart

A run chart illustrates the progression of the data throughout the time of observation. Horizontal lines represent the minimum required strengths of 4 MPa (580 psi) for f_1 and f^D_{600} and 3.7 MPa (540 psi) for f^D_{300} and f^D_{150}. These lines were added to the run chart, as shown in Fig. 5, to identify the unacceptable level of flexural strength values falling below the criteria. It is observed that more f^D_{600} data fail to meet the strength criteria than the first crack (f_1) and peak strength (f_P) (refer to Fig. 5(a)). The number of unqualified observations corresponding to f^D_{150} is considerably higher than f^D_{600} due to the residual strength decreasing at large deflections, which is more conducive to the peak-strength level (refer to Fig. 5(b)). Although the run chart detects the specimens that fail to meet the quality requirement, it cannot mathematically determine the stability and variability in the process compared to the neighbor observations such as CUSUM and EWMA.

Control charts

CUSUM—CUSUM control measure detects the cumulative sum of deviations of individual observations from the target value. If the target value and SD are unknown, the
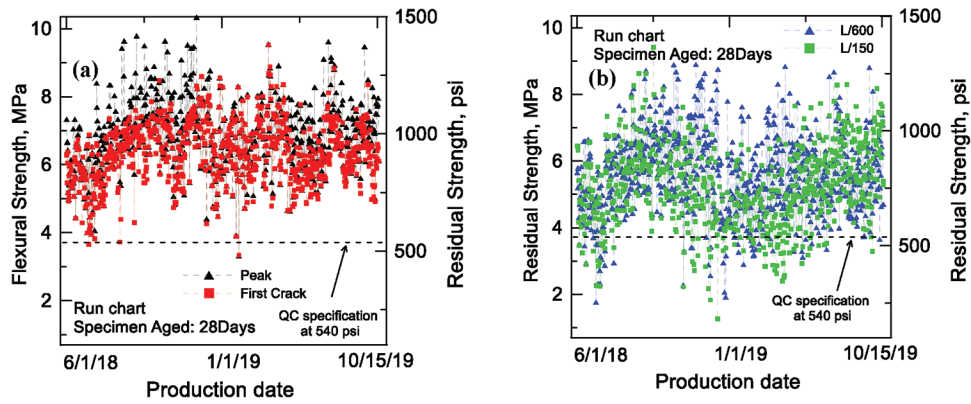
Fig. 5—Run chart of strength results over 18-month production period: (left) peak strength and first crack strength; and (right) residual flexural strength at L/150 (f^D_{150}) and L/600 (f^D_{600}).

sample population's properties can be used. The general form of the CUSUM is given by

$$C_i^+ = \max[0, x_i - (\mu_0 + K) + C_{i-1}^+]$$
$$C_i^- = \max[0, (\mu_0 + K) - x_i + C_{i-1}^-]$$
(2)

where C_i presents the CUSUM of the deviation from target values (μ_0) over the domain. A one-sided upper and lower CUSUM (above and below μ_0, respectively) are designated as C^+ and C^-. The constant $K = k\sigma$ is the reference value expressed as the SD unit adjusted by k, representing the expected sensitivity of detecting out-of-control signals in the process. The upper and lower control limits (UCL and LCL, respectively) are the horizontal lines plotted in CUSUM, defined by the decision interval term called $H = h\sigma$. In other words, the out-of-control signal is determined when C^+ exceeds UCL or C^- is below LCL. Using $k = 0.5$ and $h = 4$ provides good average run length (ARL) properties, as recommended by Montgomery.[28] Details on the evaluation of suitable values of k and h are extensively explained in earlier publications.[27,28]

The CUSUM method with resetting C^+ and C^- was used. In this study, the mean flexural strength for each scheme was assigned as the target value μ_0. The design specified strengths of 3.7 and 4 MPa (540 and 580 psi) as target values are unreasonable because the concrete was designed with a safety factor to be superior to the required residual strength. Therefore, most of the data exceeded the specified value. Use of the design-specified strength as the target value results in many out-of-control results overestimating the target value, or a large C^+ value compared to the mean value.

A key feature of the process is to reset the CUSUM every time the out-of-control signal is triggered. This is because a misleading signal may occur when the previous CUSUM was not reset to zero (that is, $C_{i-1}^- = 0$, $C_{i-1}^+ = 0$) after an out-of-control signal detection in an earlier observation. The comparison between the CUSUM chart with and without resetting the signal for the peak strength (f_p) is in Fig. 6. When $i = 7$, C^- was below UCL, and C^- at $i = 8$ was calculated without reset $C_{i-1}^- = 0$, the CUSUM in observations between 8 and 20 determined biased results below LCL. In comparison, the signal with zero resets can indicate the stability in the process independently from the process

data before an earlier outbreak signal. More discussion on using a CUSUM chart in production can be consulted in ACI 214R-11,[29] which provides examples of applying the CUSUM chart and discusses some of the difficulties with the CUSUM analysis.

EWMA—The EWMA control chart is another approach to monitoring small shifts in the data. By using an exponential weight function, EWMA gives a higher priority to a signal based on the nearby (newer) observations rather than farther neighbors (older). A typical equation is given by

$$z_i = \lambda \sum_{j=0}^{i-1}(1-\lambda)^j x_{i-j} + (1-\lambda)^i z_0$$
(3)

where $\lambda \sum_{j=0}^{i-1}(1-\lambda)^j x_{i-j}$ is the weight assigned to the neighbor observations; and the second term represents the most recent sample. The weight factor for each observation is illustrated in Fig. 7 with the value of λ used to weigh an average from neighbor observations. When $\lambda = 0.3$, a higher contribution is assigned to the closer (newer) observations, while farther (older) observations have less contribution compared to $\lambda = 0.1$ and 0.2. The smaller shift corresponds to the smaller λ assigned. UCL and LCL of the EWMA chart are identified in Eq. (4). In this study, L was defined as 3 and $\lambda = 0.3$. The appropriate values of the λ and L parameters for the control chart can be determined by ARL, which is explained in past studies.[27,28] The process detects an out-of-control signal when the EWMA exceeds the UCL and LCL.

$$\text{UCL} = \mu_0 + L\sigma\beta \text{ and LCL} = \mu_0 - L\sigma\beta;$$
$$\text{where } \beta = \sqrt{\frac{\lambda}{2-\lambda}[1-(1-\lambda)^{2i}]}$$
(4)

Interpolation of control charts—A preliminary analysis presented earlier in this paper confirmed that flexural strength at the first crack (f_1) and residual flexural strengths of f^D_{600}, f^D_{300}, and f^D_{150} all follow a normal distribution trend. An analytical investigation was conducted based on hybrid CUSUM and EWMA control chart methodology. For CUSUM, the constant values were taken as $h = 4$ and $k = 0.5$. The CUSUM method with resetting C^+ or C^- was adopted. The EWMA control chart was applied with the constant
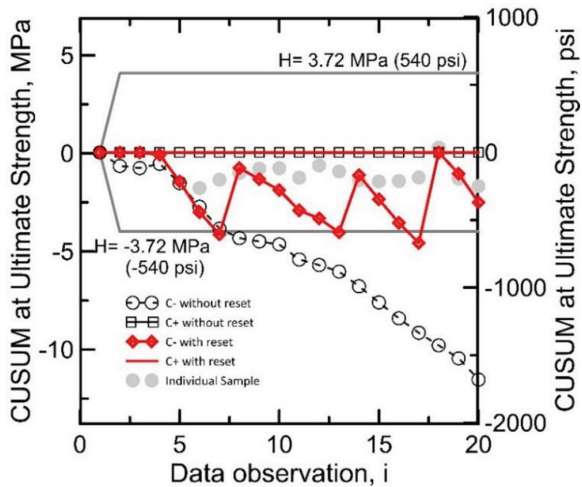
Fig. 6—CUSUM with and without reset when signal exceeds limit for peak strength, f_p.

Fig. 7—Comparison of weight factor of CUSUM and EWMA.

value of $L = 3$ and $\lambda = 0.3$. The mean value of flexural strength for each scheme was assigned as the target value μ_0.

The control charts are investigated in Fig. 8 to 12 by adopting the constant parameters described earlier for flexural strength at various stages. Several aspects of the control chart in addressing the variations in the process become apparent by evaluating it in conjunction with the run chart in the form of CUSUM or EWMA. The constant (horizontal) lines represent the minimum specified strength of 3.7 MPa (540 psi) for f_1 and f^D_{600}, and 4 MPa (580 psi) for f_p, f^D_{300}, and f^D_{150}. Out-of-control signals were detected in the first crack strength, f_1, from observations 1 to 150 on CUSUM and EWMA control charts, but no individual f_1 data failed to meet the required strength of 3.7 MPa (540 psi). EWMA charts do not present any out-of-control signal for other strength parameters in this observation range. CUSUM charts, except for one or two sporadic out-of-control signals for f_p and f^D_{600}, show similar results. Also, except for one single unqualified f^D_{150} test result, all other data meet specified strength in this observation range. In this case, the manufacturing process is unstable, but the concrete batch is acceptable as there is no need to be rejected. However, an investigation may be required to address the assignable causes of instability in the production process.

For observations 450 to 550, parameters f_1 and f_p indicate the out-of-control signals. While no single f_1 and f_p datum in this observation range fell under the specified strength level, f^D_{600}, f^D_{300}, and f^D_{150} reveal several unqualified strengths data. The largest number of unqualified strength specimens was found for parameter f^D_{150}. This can be explained by the fact that the flexural strength of SFRC in a conventional fiber dosage gradually decreases after f_p, and f^D_{150} is typically lower than f^D_{300} and f^D_{600}. This attributes those batches to an incapable process at an unacceptable level of strength. Similarly, observations 300 to 450 indicate out-of-control signals concerning the LCL on EWMA charts for f^D_{600}, f^D_{300}, and f^D_{150}. Also, the largest number of unqualified f^D_{600}, f^D_{300}, and f^D_{150} parameters can be seen in this observation range. The manufacturing process during such periods should be further
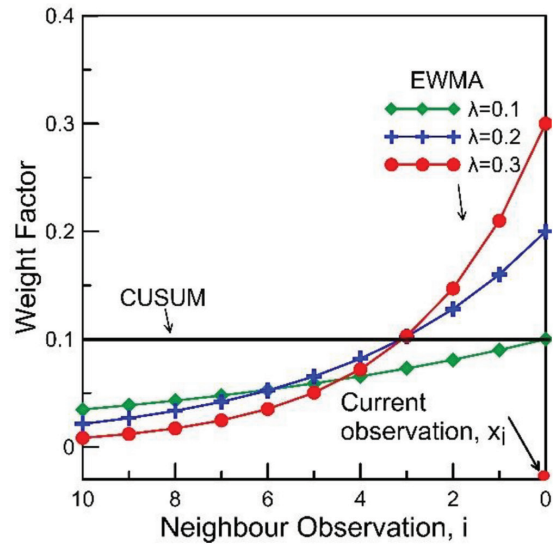
investigated for the assigned causes and corrected to be back into control before the continuous production operation may proceed. Considering out-of-control signals in observations 450 to 550 were detected for f_1 and in the observation range of 300 to 450 were detected for residual strength parameters (f^D_{600}, f^D_{300}, and f^D_{150}), it can be speculated that the assignable causes for the former range can be related to concrete and for the latter to the fiber reinforcement.

The control chart cannot be independently used as a measure of quality. Observations in the range of 200 to 300 in the EWMA control chart did not present an out-of-control signal in f_1 and f_p (refer to Fig. 8 and 10). However, several unqualified samples in residual strength fell below the required strength. This scenario shows that the manufacturing process is stable, but the samples are unqualified and need to be rejected. However, a small range of out-of-control signals was still detected within an observation range of 200 to 300 in the CUSUM chart (refer to Fig. 8 to 12), while EWMA did not support such a decision. A similar investigation found that other CUSUM charts are more sensitive to indicating the out-of-control signal compared to EWMA. This can be due to the parameters employed in the applicable formulas. It is noted that the control chart also results in a false alarm. The ARL is technically adopted to evaluate the performance of constant parameters used in the control chart. This topic is beyond the purpose of the present study and the details of ARL can be found elsewhere.[28]

MINIMUM SAMPLING REQUIREMENTS FOR ASTM C1609 TESTING

The method of random sampling can be used to estimate the minimum required sample size with an acceptable design variability. The distribution of fibers is a random process and primarily a function of orientation and the number of fibers at the cracked section. This leads to varying post-crack strength and causes a high COV. These characteristic values of FRC may require testing of a higher number of samples to gain a reliable distribution of flexural strength parameters representing the population data set.
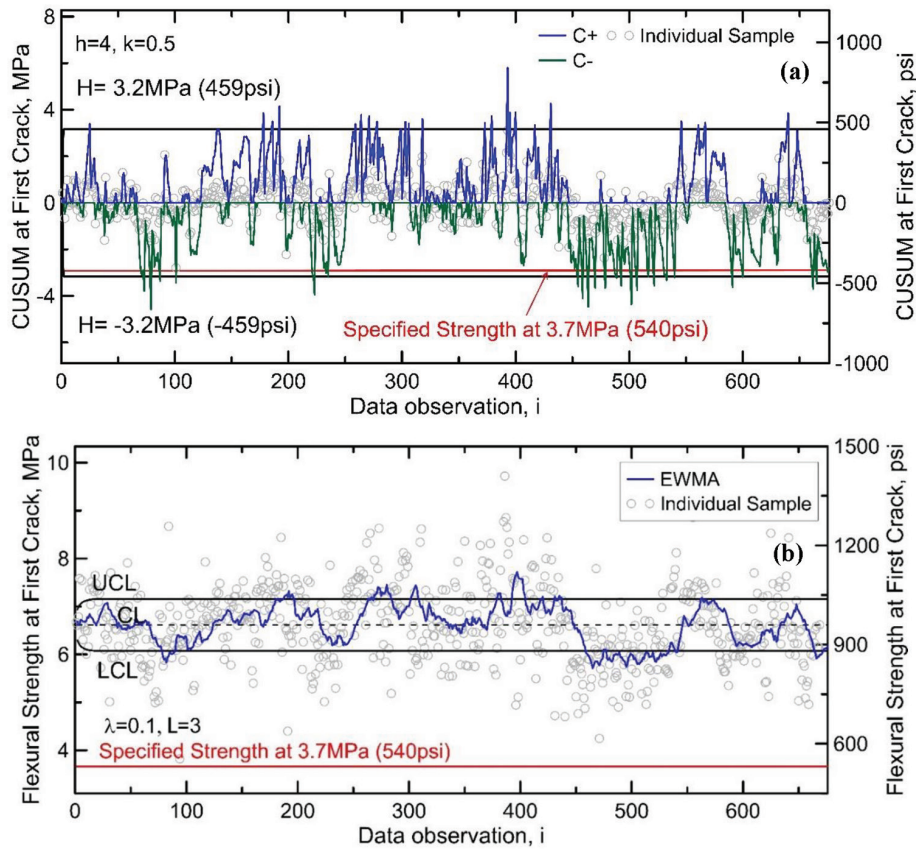
Fig. 8—Control charts of first crack strength (f₁) at 28 days collected from June 2018 to October 2019: (top) CUSUM; and (bottom) EWMA.
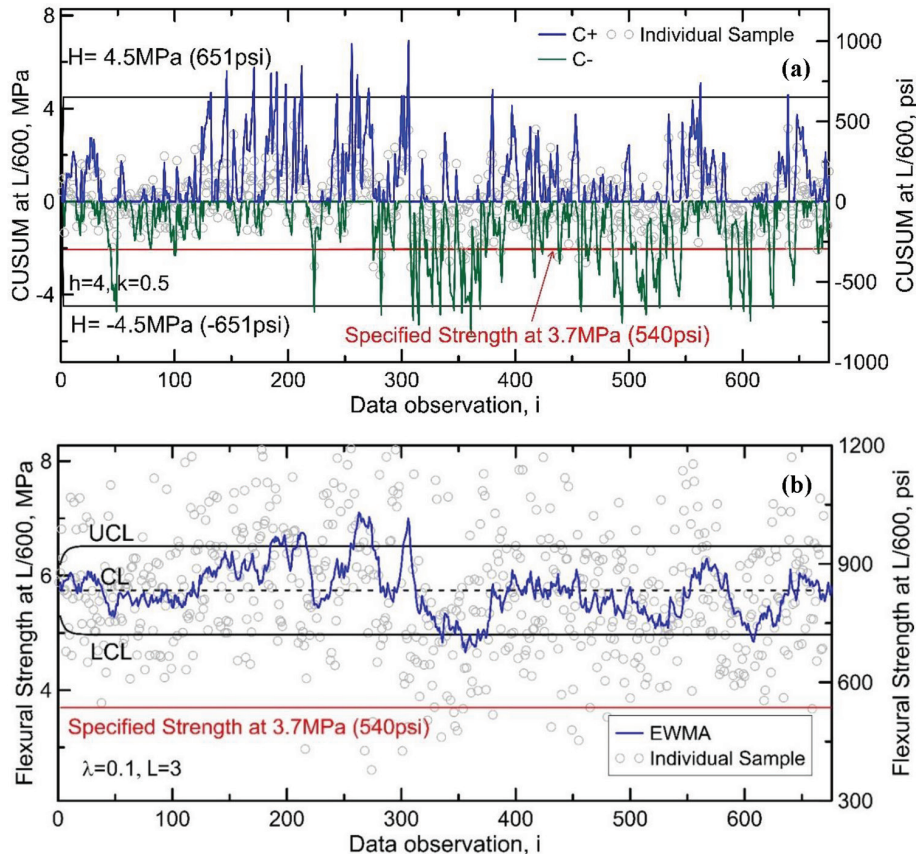

Fig. 9—Control charts of residual strength at L/600 (f$^D_{600}$) at 28 days collected from June 2018 to October 2019: (top) CUSUM; and (bottom) EWMA.
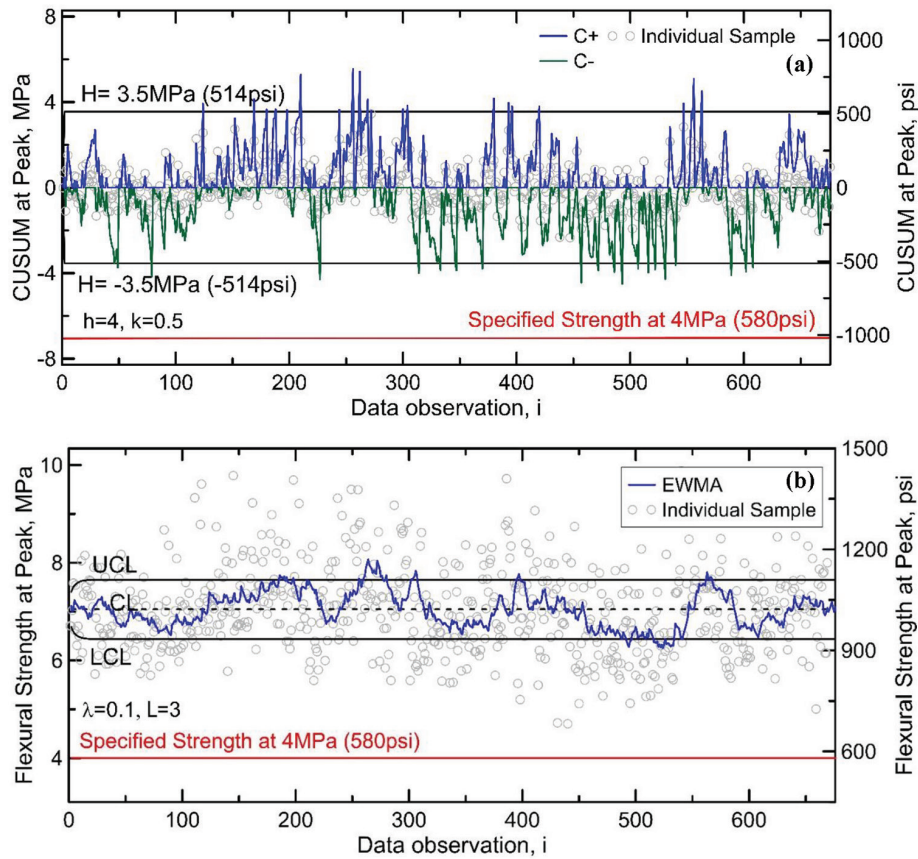
Fig. 10—Control charts of residual strength at peak strength (f_p) at 28 days collected from June 2018 to October 2019: (top) CUSUM; and (bottom) EWMA.
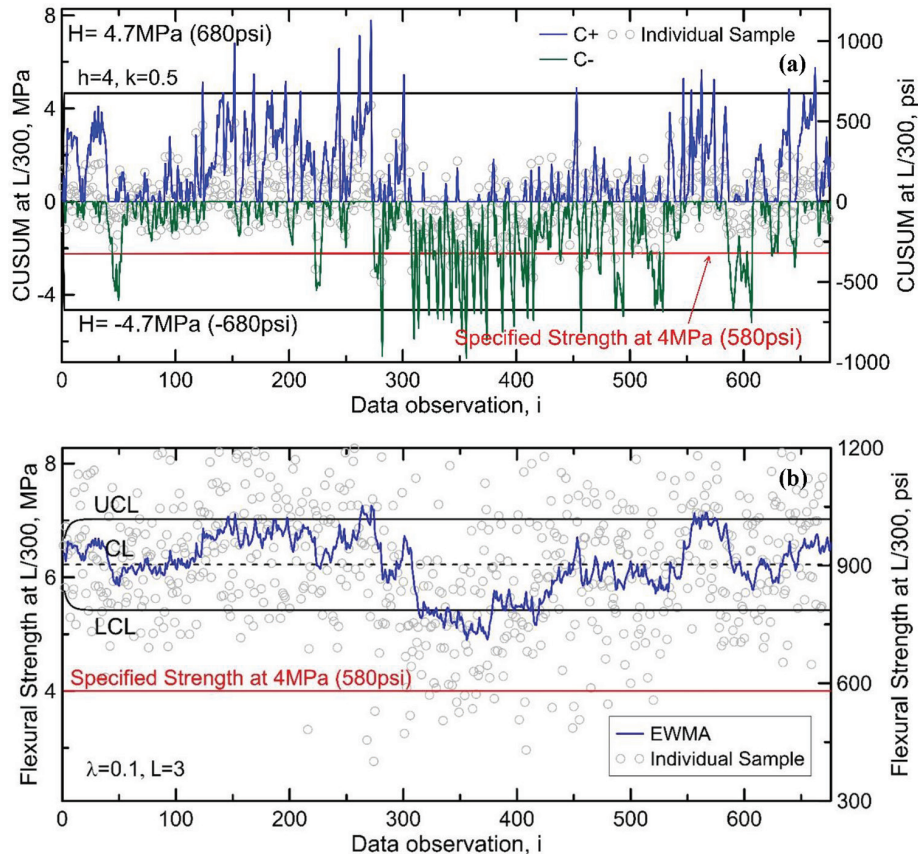

Fig. 11—Control charts of residual strength at L/300 (f^D_{300}) at 28 days collected from June 2018 to October 2019: (top) CUSUM; and (bottom) EWMA.
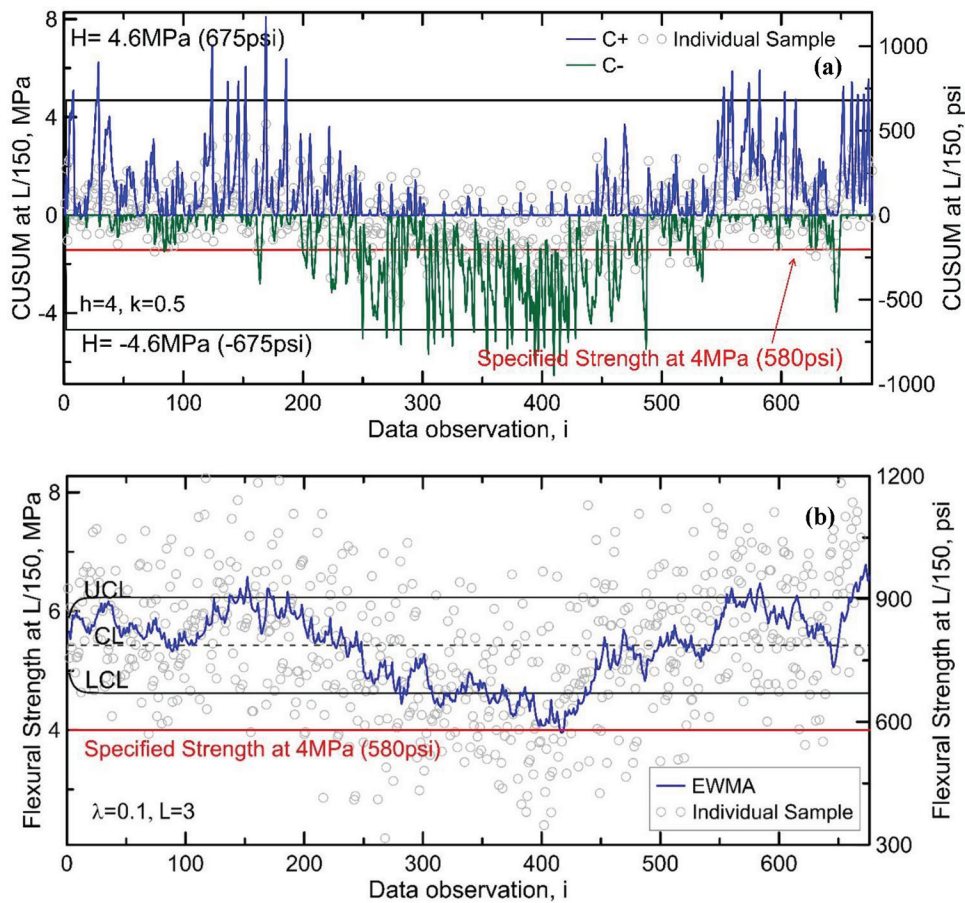
Fig. 12—Control charts of residual strength at L/150 (f^D_{150}) at 28 days collected from June 2018 to October 2019: (top) CUSUM; and (bottom) EWMA.

Among the entire data, a method by random resampling of the data with replacement, known as the Bootstrap Method, was adopted for simulation and assigning accuracy measures of the statistical estimates. This method evaluates the standard error in any statistical measure such as the mean, median, and SD by randomly sampling from a pool of sample data that are a part of the same population.[30] This method ensures that the variability measure is independent of the date or process of manufacturing and can have wider implications in terms of expected error in a sample size considering limited testing capabilities. The Bootstrap approach could also be used to measure errors in other statistical estimates for which analytical equations are not available.

A test data recorded for $N = 701$ beams at the production of every batch was selected as the population data set. The beam data excludes the 116 beam samples that did not reach L/150 deflection point from the total 817 beams. The flexural strength at first cracking, f_1, and the residual strengths f^D_{600}, f^D_{300}, and f^D_{150} were selected as primary parameters of interest. The process requires the selection of "n" random samples from the population data, referred to the Bootstrap sample set and denoted by a vector $X_m = (x_1, x_2, \ldots, x_n)$, where n is the sample size and m denotes the trial set. The sampling of each data point is done independently with replacement from the population data pool, meaning every one of n values has an equal probability of $1/N$. The sample

mean $\bar{x}$ and sample SD s of each Bootstrap sample set are recorded at every trial. This process can be conducted for any number of trials, and in this case, was repeated for $m = 50$ trial sets. The process was then repeated with higher and higher sample sizes, with n ranging from 3 to 500.

Figure 13 presents the 95% two-sided CIs of the Bootstrap samples of size n with the bond lines and the mean of the sample means ($\bar{x}$) of all $m = 50$ trials with solid lines, as well as the tracks line of population mean. The CI can be interpreted as, 95% of the time, the variation in the sample means will fall under the shaded area. As the number of samples n in the Bootstrap sample increases, the variability in the sample means decreases as expected. It was observed that moving from a sample size of three to five, the 95% CI reduces by 20 to 28%, and a further reduction of approximately 20 to 40% is observed when moving from sample size five to 10. It is also observed that the 95% two-sided CI reaches stability near the Bootstrap sample size of $n = 100$. Compared to the first-crack strength (f_1) and other residual strength parameters in Fig. 13(b), f^D_{150} shows a wider scatter of 95% CI when a sample size of 10 or less is selected, showing lower reliability on measured strength parameters when a small sample size is available. This study provides an insight into the accuracy of the sample mean as the size varies and shows that given the type of distribution, a smaller sample can represent the mean as accurately as the entire population, considering that the measured average
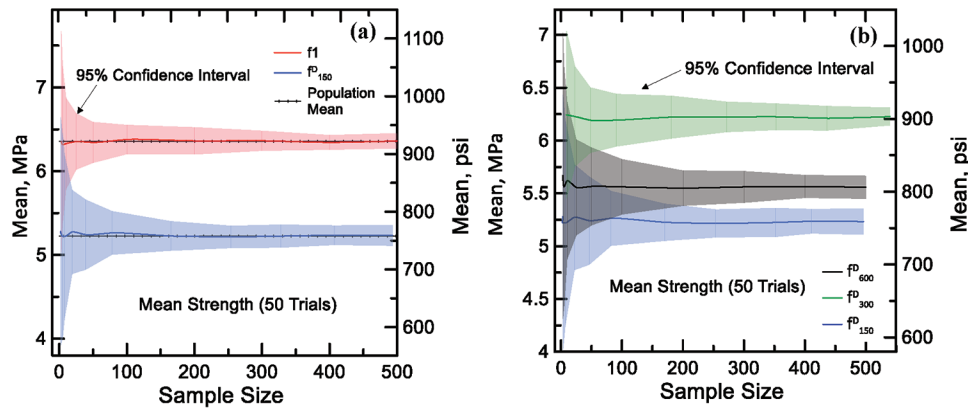
Fig. 13—Interval plots of sample size versus mean using random sampling and Bootstrap analysis of ASTM C1609 strength parameters: (left) 95% CIs for first crack strength and residual strength at L/150 deflection; and (right) 95% CIs for various residual strength parameters.
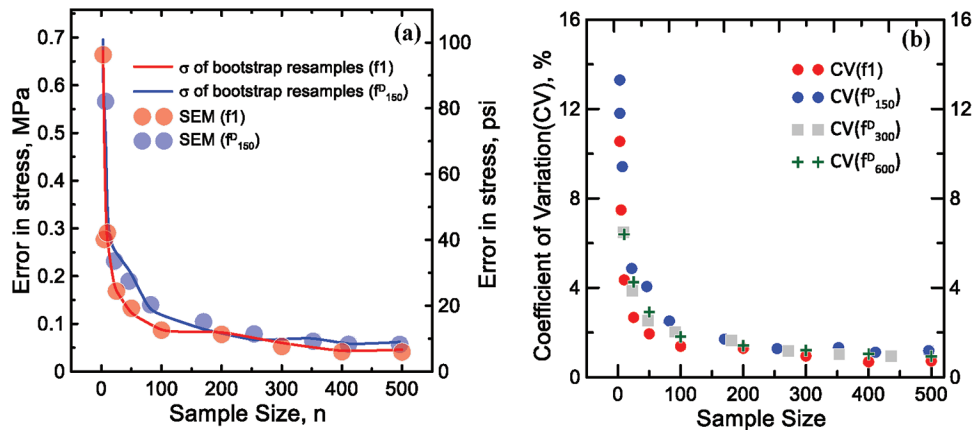

Fig. 14—(left) Comparison of SD from Bootstrap analysis versus analytical SEM; and (right) comparing coefficient of variation in bootstrap samples.

value should be factored for expected error, also referred to as "standard error". The study also provides estimates of the number of samples required for higher accuracy in test data with the associated errors.

A simpler and traditional analytical method is referred to as standard error of mean (SEM) as the statistical estimate of accuracy, and defined as $s/\sqrt{n}$, with s as the sample SD of sample size and n as the number of samples. Figure 14(a) compares the traditional approach with the simulated resampling approach of bootstrapping. Both approaches show similar accuracies in mean strength deviations and estimating errors as a function of sample size.

The COV, defined as COV = σ/μ, is another statistical parameter used with the bootstrapping method. The COV for all residual strength parameters is plotted in Fig. 14(b). The COV in parameter f^D_{150} is 13.2% for a sample size of $n = 3$, and 11.8% for a sample size of $n = 5$. Around $n = 25$ samples are required for COV to become 5% or lower, and as the sample size increases above 100, the COV reduces significantly to 2.5%, and remains stable below 1.5% for sample sizes greater than 200. Appropriate variability factors can be derived from the COV for specific sample size and strength parameters. The other strength parameters (f^D_{600} and f^D_{300}) indicated a similar tendency of COV, as illustrated in Fig. 14(b).

The COV and confidence interval charts can be used to select the minimum required sample size to characterize the entire population of FRC or to evaluate QC parameters for different suppliers. It can be used to determine the required number of standard ASTM C1609 or EN 14651 tests to meet the design properties of FRC. Note that the measured variation of strength is specific for a single fiber type as well as dosage in this study, and the measured errors with respect to sample size may change with different fiber types and their properties. The presented study, however, can be easily extended to other groups of fibers, and similar conclusions are expected to be drawn.

CONCLUSIONS

Residual flexural strength is primarily a design parameter that controls the serviceability and strength of structural fiber-reinforced concrete (FRC) elements such as precast tunnel segments. High variability in the manufacturing process is inevitable in FRC structures, especially in full-scale specimens; therefore, suitable safety for the manufacturing process needs to be implemented. The descriptive statistics were calculated, and the highlighted information was drawn here. The Anderson-Darling (AD) approach fit of the distribution indicated that the data is best described by a normal distribution as compared to lognormal and Weibull

distribution. The scatter range of 28-day specimens ranged from a minimum load of 14 kN (3108 lb) to a maximum load of 77 kN (17,232 lb). The disparity between the first crack strength and the peak strength is due to the presence of both deflection softening and deflection hardening. The deflection hardening was recorded with the mean peak strength f_P noted at 6.8 MPa (985 psi) with 95% two-sided confidence intervals (CIs) being 5.2 and 8.5 MPa (750 and 1235 psi). The mean flexural strength at first crack f_1 was 6.36 MPa (923 psi) with 95% two-sided CI values of 4.87 and 7.72 MPa (707 and 1119 psi). The similar results of residual flexural strength parameters indicate that when using basic statistics on the tested mixtures, no significant differences among the parameters are observed. Comparison of ASTM C1609's average equivalent flexural strength ($f^D_{e,150}$), calculated based on total toughness (area under load-deflection curve) with three major residual parameters at various deflection stages, indicates that f^D_{600} is the most representative residual strength parameter of the post-crack region, especially with less than a 1% difference from the mean value of $f^D_{e,150}$. The 95% lower confidence bound for all of the 28-day residual strength values f^D_{600}, f^D_{300}, and f^D_{150} of the FRC mixtures were 4.87, 3.73, and 3.98 MPa (707, 541, and 577 psi). Because these values are larger than the design parameters, they validate the selection of FRC mixture.

The statistical process control (SPC) procedures used a combination of the run chart, exponentially weighted moving average (EWMA), and cumulative sum (CUSUM) control charts to identify spurious shifts (or out-of-control signal) in the mean values of flexural strengths. Results show that the tendency in the residual strength parameters is to decrease at large deflections; hence, the number of unqualified observations corresponding to the end deflection stage is considerably higher than the strength reported at early stages of post-crack response, which are more conducive to the peak strength levels. Periods with incapable manufacturing processes at an unacceptable level of strength were identified for further examination to move the process back into control before the continuous production operation may proceed.

The Bootstrap Method applied to the data determined the minimum required number of samples to test for a specific level of variance to match the population variance. The coefficient of variation (COV) and CI charts were introduced and show that a sample set of 25 specimens could provide a reasonable level of estimation for flexural strength parameters with COV = 5% or less. The 95% two-sided CI was observed to reach stability after selecting a sample close to 100. This indicates that the frequency of the quality control (QC) data collection can be reduced significantly without a significant impact on the overall analysis of the results.

AUTHOR BIOS

Chidchanok Pleesudjai was a Graduate Research Assistant at the School of Sustainable Engineering and the Built Environment, Arizona State University (ASU), Tempe, AZ. She received her BEng in civil engineering from Chulalongkorn University, Bangkok, Thailand, in 2015 and her MS in structural and materials engineering from ASU in 2021. Her research interests include analytical solutions for serviceability-based flexural design of fiber-reinforced concrete.

Devansh Patel is a Graduate Research Assistant at the School of Sustainable Engineering and the Built Environment at ASU. He received his BS in civil engineering from University of Pune, Pune, India, in 2017 and his MS in structural and materials engineering from ASU in 2020. His research interests include fiber-reinforced cement composites and their application in tunnel linings.

Kenneth A. Williams Gaona was a Graduate Research Assistant at the School of Sustainable Engineering and the Built Environment at ASU. He received his BS in civil engineering from Santa María La Antigua Catholic University, Panama City, Panama, in 2017 and his MS in structural and materials engineering from ASU in 2020. His research interests include fiber-reinforced cement composites and their application in tunnel linings.

ACI member **Mehdi Bakhshi** is a Lead Tunnel Engineer at AECOM. He received his BS and MS in civil and structural engineering from the University of Tehran, Tehran, Iran, and his PhD in civil, environmental and sustainable engineering from ASU. He is a member of ACI Committees 305, Hot Weather Concreting; 350, Environmental Engineering Concrete Structures; 506, Shotcreting; 533, Precast Panels; and 544, Fiber Reinforced Concrete. His research interests include structural design and tunnel engineering.

ACI member **Verya Nasri** is Chief Tunnel Engineer at AECOM. He received his BS and MS in structural engineering from Sharif University of Technology, Tehran, Iran, and his PhD in geotechnical engineering from École Centrale Paris, Châtenay-Malabry, France. His research interests include geotechnical, structural, and tunnel engineering, including design and construction support for major tunneling projects.

Barzin Mobasher, FACI, is a Professor of structural materials at ASU. His publications include two books on fiber- and textile-reinforced concrete, four edited books, and more than 200 research papers. He is a past Chair and member of ACI Committee 544, Fiber Reinforced Concrete, and is a member of the ACI Technical Activities Committee; ACI Committee 549, Thin Reinforced Cementitious Products and Ferrocement; ACI Subcommittee 239-C, Structural Design on UHPC; and Joint ACI-ASCE Committee 446, Fracture Mechanics of Concrete.

REFERENCES

1. ACI Committee 544, "Report on Design and Construction of Fiber-Reinforced Precast Concrete Tunnel Segments (ACI 544.7R-16)," American Concrete Institute, Farmington Hills, MI, 2016, 36 pp.

2. Plizzari, G. A., and Tiberti, G., "Steel Fibers as Reinforcement for Precast Tunnel Segments," *Tunnelling and Underground Space Technology*, V. 21, No. 3-4, 2006, pp. 438-439. doi: 10.1016/j.tust.2005.12.079

3. Yao, Y.; Bakhshi, M.; Nasri, V.; and Mobasher, B., "Interaction Diagrams for Design of Hybrid Fiber-Reinforced Tunnel Segments," *Materials and Structures*, V. 51, No. 1, 2018, p. 35. doi: 10.1617/s11527-018-1159-2

4. Meda, A.; Rinaldi, Z.; Spagnuolo, S.; De Rivaz, B.; and Giamundo, N., "Hybrid Precast Tunnel Segments in Fiber Reinforced Concrete with Glass Fiber Reinforced Bars," *Tunnelling and Underground Space Technology*, V. 86, 2019, pp. 100-112. doi: 10.1016/j.tust.2019.01.016

5. ACI Committee 544, "Guide for Design with Fiber-Reinforced Concrete (ACI 544.4R-18)," American Concrete Institute, Farmington Hills, MI, 2018, 44 pp.

6. Molins, C., and Arnau, O., "Experimental and Analytical Study of the Structural Response of Segmental Tunnel Linings based on an In Situ Loading Test. Part 1: Test Configuration and Execution," *Tunnelling and Underground Space Technology*, V. 26, No. 6, 2011, pp. 764-777. doi: 10.1016/j.tust.2011.05.002

7. Bakhshi, M., and Nasri, V., "Design of Precast Concrete Segmental Lining for the Montreal Express Link (REM) Airport Tunnel," *ITA-AITES World Tunnel Congress and 46th General Assembly*, Kuala Lumpur, Malaysia, May 15-21, 2020.

8. Bakhshi, M., and Nasri, V., "Crack Width Simulation and Nonlinear Finite Element Analysis of Bursting and Spalling Stresses in Precast FRC Tunnel Segments Under TBM Thrust Jack Forces," *Fibre Reinforced Concrete: Improvements and Innovations: RILEM-fib International Symposium on FRC (BEFIB) in 2020*, P. Serna, A. Llano-Torre, J. R. Martí-Vargas, and J. Navarro-Gregori, eds., Springer, Cham, Switzerland, 2021, pp. 621-638. doi: 10.1007/978-3-030-58482-5_56

9. Cavalaro, S. H. P.; Blom, C. B. M.; Aguado, A.; and Walraven, J. C., "New Design Method for the Production Tolerances of Concrete Tunnel Segments," *Journal of Performance of Constructed Facilities*, ASCE, V. 26, No. 6, 2012, pp. 824-834. doi: 10.1061/(ASCE)CF.1943-5509.0000291

10. Buratti, N.; Ferracuti, B.; and Savoia, M., "Concrete Crack Reduction in Tunnel Linings by Steel Fibre-Reinforced Concretes," *Construction and Building Materials*, V. 44, 2013, pp. 249-259. doi: 10.1016/j.conbuildmat.2013.02.063

11. Bakhshi, M.; Barsby, C.; and Mobasher, B., "Back-Calculation of Tensile Properties of Strain Softening and Hardening Cement Composites," *High Performance Fiber Reinforced Cement Composites 6*, G. J. Parra-Montesinos, H. W. Reinhardt, and A. E. Naaman, eds., Springer, Dordrecht, the Netherlands, 2012, pp. 83-90. doi: 10.1007/978-94-007-2436-5_11

12. Mobasher, B., *Mechanics of Fiber and Textile Reinforced Cement Composites*, first edition, CRC Press, Boca Raton, FL, 2011.

13. Nguyen, D.-L.; Thai, D.; Ngo, T.; Tran, T.; and Nguyen, T., "Weibull Modulus from Size Effect of High-Performance Fiber-Reinforced Concrete under Compression and Flexure," *Construction and Building Materials*, V. 226, Nov, 2019, pp. 743-758. doi: 10.1016/j.conbuildmat.2019.07.234

14. Yoo, D.; Banthia, N.; Yang, J.; and Yoon, Y., "Size Effect in Normal- and High-Strength Amorphous Metallic and Steel Fiber Reinforced Concrete Beams," *Construction and Building Materials*, V. 121, Sept. 2016, pp. 676-685. doi: 10.1016/j.conbuildmat.2016.06.040

15. Tiberti, G.; Germano, F.; Mudadu, A.; and Plizzari, G. A., "An Overview of the Flexural Post-Cracking Behavior of Steel Fiber Reinforced Concrete," *Structural Concrete*, V. 19, No. 3, 2018, pp. 695-718. doi: 10.1002/suco.201700068

16. Conforti, A.; Tiberti, G.; Plizzari, G. A.; Caratelli, A.; and Meda, A., "Precast Tunnel Segments Reinforced by Macro-Synthetic Fibers," *Tunnelling and Underground Space Technology*, V. 63, 2017, pp. 1-11. doi: 10.1016/j.tust.2016.12.005

17. Galeote, E.; Picazo, Á.; Alberti, M. G.; de la Fuente, A.; Enfedaque, A.; Gálvez, J. C.; and Aguado, A., "Statistical Analysis of an Experimental Database on Residual Flexural Strengths of Fiber Reinforced Concretes: Performance-Based Equations," *Structural Concrete*, V. 23, No. 5, 2022, pp. 3140-3153. doi: 10.1002/suco.202100416

18. ASTM C1609/C1609M-19, "Standard Test Method for Flexural Performance of Fiber-Reinforced Concrete (Using Beam With Third-Point Loading)," ASTM International, West Conshohocken, PA, 2019.

19. ACI Committee 544, "Report on Indirect Method to Obtain Stress Strain Response of Fiber-Reinforced Concrete (FRC) (ACI 544.8R-16)," American Concrete Institute, Farmington Hills, MI, 2016, 22 pp.

20. Mobasher, B.; Yao, Y.; and Soranakom, C., "Analytical Solutions for Flexural Design of Hybrid Steel Fiber Reinforced Concrete Beams," *Engineering Structures*, V. 100, Oct, 2015, pp. 164-177. doi: 10.1016/j.engstruct.2015.06.006

21. Sullivan, J., and Perham, A., "Design and Construction of the South Hartford CSO Tunnel," *Pipelines 2018: Planning and Design - Proceedings of Sessions of the Pipelines 2018 Conference*, 2018, pp. 69–80. doi: 10.1061/9780784481646.008

22. Bakhshi, M., and Nasri, V., "Design of Steel Fiber-Reinforced Concrete Segmental Lining for the South Hartford CSO Tunnel," *Proceedings, Rapid Excavation Tunneling Conference*, San Diego, CA, 2017, pp. 706-717.

23. *fib*, "*fib* Model Code for Concrete Structures 2010," Fédération Internationale du Béton, Lausanne, Switzerland, 2013.

24. Conforti, A.; Minelli, F.; Plizzari, G. A.; and Tiberti, G., "Comparing Test Methods for the Mechanical Characterization of Fiber Reinforced Concrete," *Structural Concrete*, V. 19, No. 3, 2018, pp. 656-669. doi: 10.1002/suco.201700057

25. Dean, S. W.; Bernard, E. S.; and Xu, G. G., "Statistical Distribution of Fiber-Reinforced Concrete Beam Test Data," *Journal of ASTM International*, V. 4, No. 3, 2007, p. 100774. doi: 10.1520/JAI100774

26. Alberti, M. G.; Enfedaque, A.; Gálvez, J. C.; and Agrawal, V., "Reliability of Polyolefin Fibre Reinforced Concrete beyond Laboratory Sizes and Construction Procedures," *Composite Structures*, V. 140, Apr, 2016, pp. 506-524. doi: 10.1016/j.compstruct.2015.12.068

27. Laungrungrong, B.; Mobasher, B.; and Montgomery, D., "Development of Rational Pay Factors Based on Concrete Compressive Strength Data," Arizona Department of Transportation, Phoenix, AZ, 2008.

28. Montgomery, D. C., "Introduction to Statistical Quality Control," *The Statistician*, V. 35, No. 1, 1986, pp. 81-82. doi: 10.2307/2988304

29. ACI Committee 214, "Guide to Evaluation of Strength Test Results of Concrete (ACI 214R-11)," American Concrete Institute, Farmington Hills, MI, 2011, 16 pp.

30. Efron, B., and Tibshirani, R. J., *An Introduction to the Bootstrap*, Chapman and Hall/CRC, Boca Raton, FL, 1994.